

# **Geophysical Research Letters**\*

# ب

#### RESEARCH LETTER

10.1029/2025GL116017

#### **Special Collection:**

Science from the Surface Water and Ocean Topography Satellite Mission

#### **Key Points:**

- The Surface Water and Ocean Topography (SWOT) mission provides two-dimensional maps of surface wind speed at 2 km resolution
- In the Gulf Stream and the Kuroshio Extension, we observe the imprint of sea surface temperature anomalies on surface winds at submesoscales
- SWOT is able to detect air-sea interactions down to a few kilometers

#### **Supporting Information:**

Supporting Information may be found in the online version of this article.

#### Correspondence to:

G. Lapeyre, guillaume.lapeyre@sorbonne-universite.fr

#### Citation:

Kaouah, M., Lapeyre, G., Renault, L., Perrot, X., & Dablemont, C. (2025). Submesoscale air-sea interactions as revealed by SWOT. *Geophysical Research Letters*, 52, e2025GL116017. https://doi. org/10.1029/2025GL116017

Received 8 APR 2025 Accepted 11 SEP 2025

#### **Author Contributions:**

Conceptualization: G. Lapeyre
Data curation: X. Perrot
Formal analysis: M. Kaouah, G. Lapeyre,
C. Dablemont
Funding acquisition: G. Lapeyre,
L. Renault
Investigation: M. Kaouah, G. Lapeyre.

**Investigation:** M. Kaouah, G. Lapeyre, L. Renault

Methodology: M. Kaouah, G. Lapeyre

Resources: X. Perrot Software: M. Kaouah Visualization: M. Kaouah Writing – original draft: M. Kaouah,

G. Lapeyre

© 2025. The Author(s).

This is an open access article under the terms of the Creative Commons

Attribution License, which permits use, distribution and reproduction in any medium, provided the original work is properly cited.

# Submesoscale Air-Sea Interactions as Revealed by SWOT

M. Kaouah<sup>1,2</sup>, G. Lapeyre<sup>1</sup>, L. Renault<sup>2</sup>, X. Perrot<sup>1</sup>, and C. Dablemont<sup>3</sup>

<sup>1</sup>LMD-IPSL, ENS, Université PSL, Sorbonne Université, CNRS, Paris, France, <sup>2</sup>Université de Toulouse, LEGOS (CNES/CNRS/IRD/UPS), Toulouse, France, <sup>3</sup>Institut des Sciences Moléculaires d'Orsay (ISMO), CNRS, Université Paris-Saclay, Orsay, France

**Abstract** At midlatitudes, air-sea interactions have been documented in numerical models, in situ campaigns and satellite observations down to the ocean mesoscales. However little is known about scales of a few kilometers (the submesoscales). The new satellite mission Surface Water and Ocean Topography (SWOT) provides a global coverage of these scales by measuring sea surface height. Through the radar backscatter coefficient, it also provides surface wind speed at the same resolution. Here, we examine situations in the Gulf Stream and Kuroshio Extension regions where SWOT as well as scatterometer winds and sea surface temperature (SST) at kilometer scale were available. A good correspondence between winds from SWOT and scatterometer is found at the mesoscales. More importantly, the signature of SST anomalies is found in SWOT winds down to 10 km scales, confirming the effect of the ocean on the atmosphere at those scales. SWOT therefore opens new opportunities for the study of submesoscale air-sea interactions from space.

Plain Language Summary The Surface Water and Ocean Topography (SWOT) mission has been designed to monitor the global ocean at fine scales (i.e., down to a few kilometers) through the measure of sea surface height (SSH) (from which ocean currents can be computed). However, SWOT's capability is not limited to this, since it also provides other important climate variables, such as surface winds. This suggests the possibility to better understand the relation between the ocean and the atmosphere at fine scales. In the Gulf Stream and Kuroshio Extension region, using SWOT's data set as well as other satellite products, we show that there is a high correlation between sea surface temperature and winds, with low winds above cold oceanic fine scales and higher winds above warm features. Such a result agrees with theoretical mechanisms about the effect of the ocean on the atmosphere. We then conclude that SWOT is a powerful tool to document air-sea interactions at kilometer scales from space.

#### 1. Introduction

Oceanic submesoscale currents (corresponding to scales from 1 to 50 km) have received considerable attention in the last 2 decades for their non-negligible role in the climate system (see reviews by Klein and Lapeyre (2009), McWilliams (2016), and Taylor and Thompson (2023), among others). In particular, they significantly influence vertical and horizontal fluxes of heat and biogeochemical materials (Lévy et al., 2018; Su et al., 2018) and also modulate the oceanic forward and inverse energy cascades (Capet et al., 2008; Klein et al., 2008). However, the interactions of submesoscale flows with the atmosphere remain poorly understood, likely due to technical limitations such as model and satellite resolution, as well as challenges of capturing these features with ship-based campaigns (Nuijens et al., 2024). Nevertheless, growing evidence in the recent literature underscores their importance in modulating the atmospheric variability. For example, in situ data in the Western Pacific showed variations of latent heat flux of O(10) W m<sup>-2</sup> over a submesoscale front of O(5) km (Song et al., 2022). Similar observations were made in the Gulf of Mexico with variations in wind speed of 1 m s<sup>-1</sup> in relation with a variation of 1.5°C in sea surface temperature (SST) over 6 km (Shao et al., 2019). Using numerical models resolving submesoscales, Wenegrat and Arthur (2018) and Strobach et al. (2022) showed that the marine atmospheric boundary layer (MABL) actually responds to ocean features at these fine scales. As shown by Vivant et al. (2025), the response is not limited to the MABL but extends to the whole troposphere as moist convection was found to be triggered above submesoscale fronts over the passage of midlatitude storms. Other numerical studies by Sullivan and McWilliams (2022), Bai et al. (2023), and Conejero et al. (2024) revealed the effect of submesoscale ocean currents on the wind and surface heat fluxes. Satellite observations of submesoscale dynamics are until now very limited and remain a challenge (Klein et al., 2019). Standard scatterometers, whose spatial resolution is about 25 km, measure mesoscale structures only. Concerning submesoscales, a very limited number of studies exist,

KAOUAH ET AL. 1 of 11



## **Geophysical Research Letters**

10.1029/2025GL116017

Writing – review & editing: M. Kaouah, G. Lapeyre, L. Renault

such as the one by Gaube et al. (2019) using the ASTER instrument on board of the Terra satellite. With its 100 m resolution, they were able to identify a submesoscale feature with a  $13^{\circ}$ C gradient over just 15 km, along with a  $2 \text{ m s}^{-1}$  wind variation associated with it. However their study considered a specific case only, in the Gulf Stream region, and no timeseries could be performed to track the evolution of such a feature.

The Surface Water and Ocean Topography (SWOT) mission launched in December 2022 (Fu et al., 2024; Morrow et al., 2019) now provides two-dimensional maps of sea surface height (SSH) with a spatial resolution of 2 km. First studies have shown that the SWOT mission will help better characterizing submesoscale currents (Archer et al., 2025; Zhang et al., 2024). Here, our primary goal is to highlight the potential of SWOT in documenting air-sea interactions at fine scales through its associated surface wind product. To this end, we present illustrative cases in the Gulf Stream and the Kuroshio Extension regions for which high-resolution SST products and winds from conventional scatterometers were available.

#### 2. Data

At present time, wind measurements by satellite are obtained routinely from scatterometry. The nominal resolution of the three scatterometers (ASCAT) in orbit, on MetOp-A, MetOp-B, and MetOp-C, is 12.5 km. Data are provided on swaths of 550 km with two passes by day (Verhoef et al., 2012). Despite their good spatial and time coverages, the effective resolution is only about 28 km (Vogelzang et al., 2017), preventing access to submesoscales.

The SWOT satellite was originally designed to measure surface waters at scales of a few kilometers, giving access to SSH for oceanographic applications and water elevations for hydrology. Since SWOT is a Ka-band Radar Interferometer (Peral et al., 2024), it also provides measurements of ocean surface roughness (through the radar backscatter coefficient). Through the inversion of the relation between backscatter and surface winds (which drive most part of the ocean roughness), winds can be retrieved at the same resolution as SSH measurements (see JPL D-105502 (2023) and Stiles et al. (2024), for a description of the algorithm). In brief, the algorithm is designed such that wind speed is defined as a nonlinear function of the radar backscatter coefficient, significant wave height and the incidence angle of the satellite to the surface. The function is determined using ECMWF and ASCAT products over all latitudes and on several weeks. Contrary to ASCAT, SWOT data are provided on two much narrower swaths of 60 km, but with a 2 km resolution. Also the time coverage is much scarce with a repeat period of 10 or 20 days, except for the first 3 months of the mission (April–June 2023) during which specific regions of the globe were sampled once or twice daily. We take the opportunity of this new data set to see whether air-sea interaction can be detected in the range of submesoscales.

To this end, we use SST data available at 1 km resolution from the AVHRR instrument on MetOp satellites. Data are acquired on a 2,400 km swath twice daily and only available in cloud-free or rain-free regions. A difficulty is thus to have winds and SST at the same instant of time and in the same region of the ocean, which complicates statistical studies of air-sea interactions. In this paper, we will thus document some specific cases when such concomitant observations were available. We also use satellite products of Chlorophyll concentration at the ocean surface as a proxy for submesoscale structures (see e.g., Klein & Lapeyre, 2009; Lévy et al., 2018).

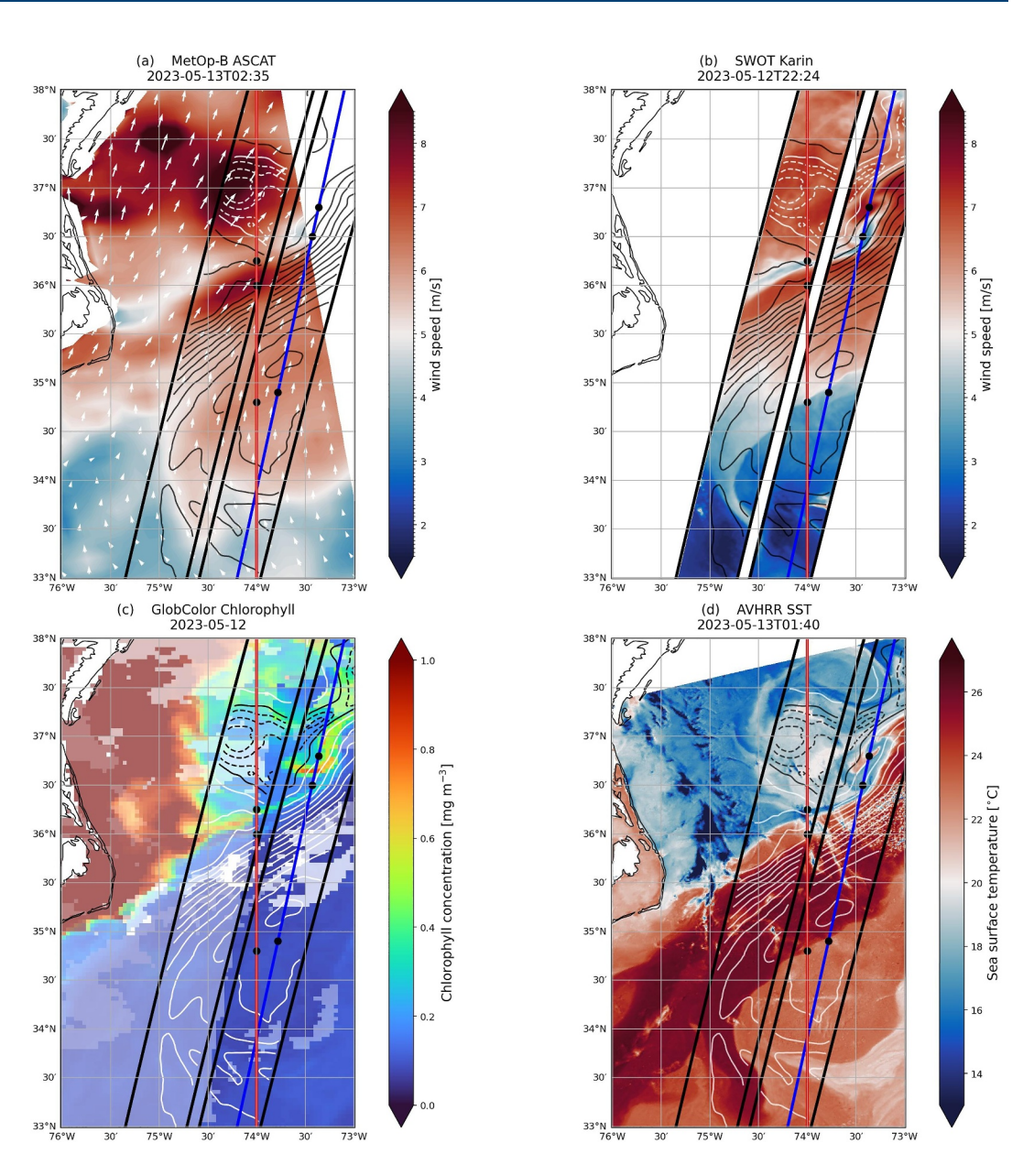
#### 3. Gulf Stream Region

Figure 1 highlights the study area near Cape Hatteras, where the Gulf Stream separates from the coast. As shown by AVHRR SST (Figure 1d), the Gulf Stream manifests itself by a pronounced SST gradient that separates warmer waters on its equatorial side from cooler waters on its poleward side. The region is also known to be characterized by strong mesoscale fronts, eddies, and submesoscale filaments and fronts (Callies et al., 2015; Gula et al., 2014). It is also prone to exceptionally strong air-sea interactions, with the largest heat transfer to the atmosphere over the global ocean (Czaja et al., 2019; Josey et al., 1999) and strong mesoscale coupling between winds and SST (Renault et al., 2019).

Figures 1a and 1b show the 10 m wind speed measured by ASCAT on 13 May 2023 at 02:35 UTC and by SWOT on 12 May 2023 at 22:24 UTC. The surface winds, as measured by ASCAT (note that SWOT does not provide wind direction), blow northward with low winds (about 4 m s $^{-1}$ ) at latitudes around 33.5°N and higher winds (about 8 m s $^{-1}$ ) poleward. This situation is similar to that studied by Sublette and Young (1996), who described a case of strong imprint of the Gulf Stream on the atmospheric boundary layer in southwesterly conditions over the

KAOUAH ET AL. 2 of 11

19448007, 2025, 20, Downloaded from https://agupubs.onlinelibrary.wiley.com/doi/10.1029/2025GL116017 by Ecole Normale Supérieure de Paris, Wiley Online Library on [21/10/2025]. See the Terms



**Figure 1.** (a) MetOp-B ASCAT wind speeds on 13 May 2023 at 02:35 UTC (with wind vectors). (b) Surface Water and Ocean Topography (SWOT) wind speed on 12 May at 22:24 UTC. (c) Chlorophyll concentration from Copernicus-GlobColor, obtained by overlaying data from 11, 12, and 13 May (see Figure S3 in Supporting Information S1 for separate figures). (d) Sea surface temperature from AVHRR on 13 May at 01:40 UTC. In panels (a–d) the same contours of absolute dynamic topography from SWOT are overlaid minus a constant value such that continuous contours correspond to anticyclones and dashed ones to cyclones. Black markers indicate six key locations that help localize features discussed in the text.

same spatial region. Additionally, comparing with Figure 1d, we note that the wind approximately blows along the SST front, which is known to favor a stronger response at both meso and submesoscales (Kilpatrick et al., 2016; Sullivan et al., 2021).

Overall, the wind speeds measured by SWOT and ASCAT are qualitatively similar to each other, except for higher winds for ASCAT in the region centered on  $34.5\,^{\circ}$ N,  $73.5\,^{\circ}$ W. A brief inspection of the ECMWF analysis at the same instant of time showed that ASCAT winds are higher than ECMWF ones as well in this region (not shown). The correlation coefficient between SWOT and ASCAT wind speeds over the spatial domain of Figure 1b is about 0.82. The spatial average of wind speed is  $5.06\,\mathrm{m\,s^{-1}}$  for SWOT against  $6.06\,\mathrm{m\,s^{-1}}$  for ASCAT while SWOT winds exhibit a higher spatial variation with a spatial r.m.s. about  $1.87\,\mathrm{m\,s^{-1}}$  for SWOT against

KAOUAH ET AL. 3 of 11

 $0.96~{\rm m~s^{-1}}$  for ASCAT. The generally lower wind speeds of SWOT compared to ASCAT could be related to the method of wind retrieval. Since the method is calibrated using data sets covering the whole globe, a point-by-point comparison may not be relevant for a particular region of space and time.

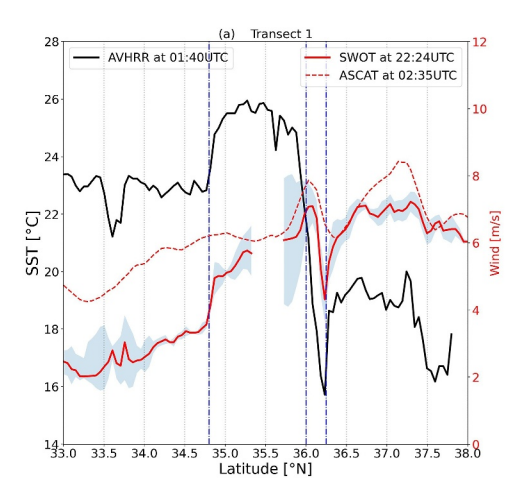
In both data sets (Figures 1a and 1b), an elongated feature with wind speeds lower than its surroundings can be observed, centered around 36.25°N, 74°W, and oriented SW-NE (identified by one of the black markers on Figure 1). Note that it is much thinner and sharper for SWOT owing its 2 km resolution against the 12.5 km resolution of ASCAT. The northeastward extension of the filament ends up around 36.5°N, 73.4°W with a roll-up of the low-wind region (see Figure S1 in Supporting Information S1, which is a close-up of this region). This feature maintains over approximately 1 day (see Figure S2 in Supporting Information S1) with maximum intensity on 12 May 2023 at 22:24 UTC. The relatively good agreement between ASCAT and SWOT at the lower range of mesoscales confirms the validity of the SWOT wind field product.

To determine how these features are related to the ocean dynamics, the spatial distribution of SST in the same region is presented on Figure 1d obtained 3 hr after the SWOT measurements which allows a direct comparison. In addition, contours of absolute dynamic topography (ADT) from SWOT are overlaid on the figure. They closely aligned with the SST fronts, providing confidence that the AVHRR SST data on 13 May at 01:40 UTC are an accurate representation of the dynamics captured by SWOT on 12 May at 22:24 UTC. A prominent tongue of warm waters (about  $\sim 26\,^{\circ}$ C) advected by the Gulf Stream extends from southwest to northeast, sharply delineating two fronts, one on its southern side, passing by 34.8°N, 74°W (corresponding to one of the black markers in Figure 1d) and one on its northern side, passing by 36°N, 74°W. Just north of it, a cold filament (centered at 36.25°N, 74°W) less than 20 km wide extends over 100 km, with Chlorophyll concentration higher than 0.4 mg m<sup>-3</sup> (Figure 1c). As the filament extends northeastward, it connects to a pouch of cold waters centered at about 36.5°N, 73.4°W (Figure 1d). This feature, about 40 km wide and with a Chlorophyll concentration as high as 1 mg m<sup>-3</sup>, is trapped between regions of warmer waters.

The spatial correspondence between AVHRR SST (Figure 1d) and SWOT wind speeds (Figure 1b) suggests that the thermal submesoscale structures have an imprint on the atmospheric winds: the elongated cold filament aligns with the minimum wind speed region, and the wrapping of submesoscale cold and warm anomalies to its northeast (centered at  $36.5^{\circ}$ N,  $73.4^{\circ}$ W and  $36.8^{\circ}$ N,  $73.4^{\circ}$ W) are similarly associated with regions of weaker and stronger winds, respectively (see also Figure S1 in Supporting Information S1 for a closer comparison). This can be further assessed by computing correlation coefficients of wind and SST anomalies at meso and at submesoscales using two-dimensional fields corresponding to Figures 1b and 1d. Anomalies are defined through a Butterworth filter of order 4 in the swath direction only as the swath is  $2 \times 60$  km wide. Using a high-pass filter with a cutoff lengthscale of 60 km, the correlation coefficient between SST and SWOT wind is 0.44 while it is equal to 0.53 applying a band-pass filter for scales 60-500 km. This confirms the visual correlation between the two fields both at meso and submesoscales. We interpret this result as a stabilization of MABL over the cold anomalies with a decrease in vertical mixing of momentum, causing a wind deceleration at the surface (Chelton et al., 2001; Hayes et al., 1989; Wallace et al., 1989). Next paragraphs will show it cannot be explained by the additional effect of ocean currents on the wind stress.

We now examine two transects to determine how SST spatial variations are concomitant with surface wind field variations (Figure 2). The first transect along the longitude 74°W (red line in Figure 1a) crosses twice the tongue of warm waters constituting the Gulf Stream at about 34.8°N and 36°N (Figure 2a). The southern front corresponds to an SST gradient of about 3°C over 5 km while the second front is much sharper with a variation from 26°C to 16°C over 10 km. The minimum of SST at around 36.25°N corresponds to the cold filament seen in Figure 1d. The wind speeds measured by SWOT are in general agreement with the ASCAT winds north of 35°N. The general underestimation of the wind by SWOT below this latitude might be related to the high temporal variability observed there. Indeed, ASCAT winds on 12 May at 15:27 UTC were also 1–2 m s<sup>-1</sup> weaker than winds on 13 May at 02:35 UTC (not shown). Concerning those latitudes, the increase in wind speed at 34.8°N measured by SWOT and absent in ASCAT is located at the same location as the SST front. This suggests that the high resolution of SWOT is able to detect fine scale variations in wind speeds which cannot be seen by ASCAT. Concerning the cold filament at 36.25°N, a wind drop of about 1.5 m s<sup>-1</sup> is measured by ASCAT over 30 km while it is sharper and stronger, with a value of more than 2 m s<sup>-1</sup> over 10 km for SWOT. The observed wind change may be an artifact of the measurement technique, as the radar interferometer KaRin on board of SWOT measures 10 m winds relative to the surface ocean currents, similar

KAOUAH ET AL. 4 of 11



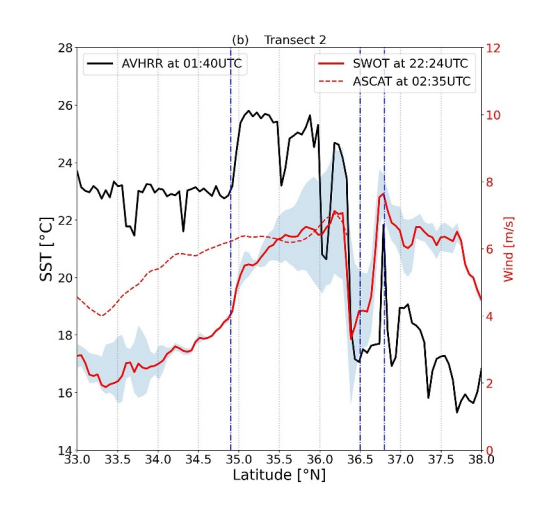


**Figure 2.** Transects of Surface Water and Ocean Topography (SWOT) and ASCAT wind speed and AVHRR sea surface temperature. Panel (a) corresponds to transect along the red line in Figure 1a and panel (b) to the blue line. The gray envelopes correspond to  $U_{SWOT} \pm 0.9U_{oce}$  with  $U_{oce}$  geostrophic ocean current provided in the SWOT products. The vertical lines correspond to the latitudes of the six markers in Figure 1.

to scatterometry. Therefore, interpreting true wind speed requires adding a correction factor for the ocean current velocity  $U_{oce}$ . But only part of the surface currents needs to be considered since there exists a direct wind response of about 10% of  $U_{oce}$  at submesoscales (Renault et al., 2024). A rough estimate of the uncertainty in wind measurements is represented by the gray envelopes on Figures 2a and 2b, corresponding to  $U_{SWOT} \pm (1-0.1)U_{oce} = U_{SWOT} \pm 0.9U_{oce}$  with  $U_{oce}$  the SWOT geostrophic current. The variation in wind at 34.8°N is in a region of weak ocean currents and the same is true for the cold filament at 36.25°N. This indicates that the submesoscale variations of the SWOT wind field at these places are related to real wind variations.

The second transect we analyze intersects the submesoscale low-wind structures visible on SWOT measurements (blue line in Figure 1b). Unfortunately, ASCAT did not cover this particular region at that time. The region with minimum wind at about  $36.5\,^{\circ}N$  (corresponding to the submesoscale pouch of cold waters) is about  $30\,\mathrm{km}$  width in both SWOT and AVHRR (Figure 2b). It corresponds to a variation of SST about  $8\,^{\circ}C$ . North of it, the SST has a peak with an increase of about  $4\,^{\circ}C$  over  $5\,\mathrm{km}$ , and a further decrease further north. This corresponds to the small-scale SST and wind anomalies visible on Figures 1b and 1d, centered at  $36.8\,^{\circ}N$  73.4 $^{\circ}W$ . Concerning wind speeds, ASCAT winds do not vary much along the transect south of  $36\,^{\circ}N$  while there is a sharp gradient of SWOT winds of about  $1.5\,\mathrm{m\,s^{-1}}$  over  $20\,\mathrm{km}$  at the location of the southern SST front at  $34.75\,^{\circ}N$  (SST increase of  $3\,^{\circ}C$ ). The cold ocean pouch at about  $36.5\,^{\circ}N$  is associated with a wind variation of about  $3\,\mathrm{m\,s^{-1}}$ , while the small-scale warm anomaly at  $36.8\,^{\circ}N$  is associated with a wind variation of about  $1.5\,\mathrm{m\,s^{-1}}$ . The effect of currents on the measured winds may be as large as  $2\,\mathrm{m\,s^{-1}}$ , but does not explain the drop of winds within the cold pouch and the increase north of it. We therefore infer that the strong wind deceleration observed in the cold pouch can be attributed to a real variation in wind speed.

Both transects have shown the strong spatial correlation of SST variations with wind variations. This strongly suggests that the ocean drives the dynamics of the MABL, conceivably through a change of the stability of the boundary layer: weaker winds above cold anomalies and stronger winds over warm anomalies. We now attempt to estimate the coupling coefficient between wind and SST at submesoscales. A first method is to use a standard regression technique using spatial anomalies. Using a Butterworth filter with a cutoff of 60 km in the swath direction on instantaneous two-dimensional fields of Figures 1b and 1d leads to a value of 0.2 m s<sup>-1</sup> °C<sup>-1</sup> at submesoscales, stronger than those obtained in numerical simulations (Conejero et al., 2024; Renault et al., 2024) which are about 0.15 m s<sup>-1</sup> °C<sup>-1</sup>. Using a band-pass filter for scales between 60 and 500 km, one obtains a value about 0.25 m s<sup>-1</sup> °C<sup>-1</sup>, corresponding to mesoscales. This value is in line with observations of O'Neill (2012) obtained from buoys in the Gulf Stream region.

KAOUAH ET AL. 5 of 11

Another method to estimate this coefficient consists in computing the ratio of the across-front variation of wind speed to the variation of SST, directly from the transects of Figure 2. This method is similar to the ones used during in situ campaigns (e.g., Shao & Wu, 2024). For the front at 34.8°N on Figure 2a, we get a typical value of about  $0.6 \text{ m s}^{-1} \, ^{\circ}\text{C}^{-1}$  (i.e.,  $2 \text{ m s}^{-1} \, ^{\circ}\text{C}^{-1}$  (i.e.,  $2 \text{ m s}^{-1} \, ^{\circ}\text{C}^{-1}$  (i.e.,  $2.5 \text{ m s}^{-1} \, ^{\circ}\text{C}^{-1}$  over 10 km) for SWOT and  $0.4 \text{ m s}^{-1} \, ^{\circ}\text{C}^{-1}$  for ASCAT. Concerning the second transect (Figure 2b), the drop over the SST pouch corresponds to a coupling coefficient of about  $0.4 \text{ m s}^{-1} \, ^{\circ}\text{C}^{-1}$ . Such values are in rough agreement with those found by Shao and Wu (2024) going up to 1 m s<sup>-1</sup>  $\, ^{\circ}\text{C}^{-1}$ .

#### 4. Kuroshio Extension Region

To generalize the findings from the Gulf Stream region, we repeat the above analysis in a different energetic region of the ocean. We choose the Kuroshio Extension region as it is a known place of strong mesoscale and submesoscale activity (Qiu, 2003; Qiu et al., 2017; Scharffenberg & Stammer, 2010). Figure 3 presents a typical case of the signature of an ocean eddy on the atmosphere. Our analysis focuses on a specific meander of the Kuroshio on 4 May 2023 (see Figure 3e). On its northern edge, a cyclonic eddy is present centered at 36.6°N, 157.6°W, associated with a negative ADT anomaly and with Chlorophyll concentration higher than 1 mg m<sup>-3</sup> (letter C in Figure 3c). It corresponds to a cold eddy, of 50 km diameter, as seen in SST on 4 May 2023 at 10:50 UTC (Figure 3d). The wind speed measured by SWOT at 19:02 UTC (Figure 3b) is in general agreement with ASCAT (at 00:01 UTC on next day, Figure 3a) at mesoscales (correlation coefficient of 0.96 over the region covered by SWOT). However it is of much smaller magnitude (6.8 m s<sup>-1</sup> against 8.9 m s<sup>-1</sup> in terms of spatial average). We do not have an interpretation of this result but note that ECMWF analysis has wind speeds magnitude consistent with SWOT (not shown). Both ASCAT and SWOT products detect the signature of the cyclonic eddy in the wind field, albeit with much smoother and weaker variations of winds for ASCAT. The SWOT wind anomaly is negative and centered above the cold eddy (Figure 3b), which suggests that the MABL is stabilized by the ocean anomaly. The coupling coefficient using a Butterworth high-pass filter of 120 km gives a value of 0.35 m s<sup>-1</sup> °C<sup>-1</sup>. This is in line with typical values found by Ma et al. (2015) for the Kuroshio Extension region.

Another example (on 28 May 2023) concerns wind variations across strong SST gradients on the periphery of ocean eddies. Figure 4e shows such a case, still in Kuroshio Extension region, with a typical SST variation of about 3.5°C over 20 km (centered at 37°N, 157°W), at the rim of a warm eddy (Figure 4d). Note here that the closest AVHRR SST field was obtained on 25 May (i.e., 3 days before) but the eddy did not move much, as can be seen when comparing with ADT contours or Chlorophyll concentration field on 28 May (Figures 4c and 4d). In this situation, the wind is blowing along the SST front, as seen in ASCAT winds (Figure 4a), a situation prone to strong air-sea interactions. For both SWOT and ASCAT there is a strong wind gradient at the periphery of the ocean eddy. However, it is much sharper for SWOT due to its higher resolution, as the wind changes by 2.5 m s<sup>-1</sup> over 10 km, while for ASCAT it changes over 50 km (not shown). Note that the strongest ADT gradients (i.e., geostrophic currents) occur westward of the wind gradient (Figure 4b). In this situation as well, the wind variations observed by SWOT are not associated with ocean currents but reflect the role of SST in stabilizing or destabilizing the MABL.

#### 5. Discussion

New opportunities are offered by the SWOT satellite mission as it measures surface wind speeds down to 2 km resolution, that is, at submesoscales, contrary to present scatterometers whose effective resolution is 28 km only. Our study, based on SWOT and other satellite observations in the Gulf Stream and the Kuroshio Extension regions, showed different situations where surface winds are correlated with SST anomalies down to a few kilometers. Such correlations suggest that processes such as downward momentum mixing (Chelton et al., 2001; O'Neill et al., 2005), pressure adjustment (Lindzen & Nigam, 1987) or the current feedback (Renault et al., 2016) are present down to submesoscales.

One first caveat is that the instantaneous imprint of the ocean on surface winds is not a general case and is not observed at any place and at any time. The synoptic atmospheric variability, such as midlatitude storms, rain cells or convective rolls, in general hinders such a signature.

KAOUAH ET AL. 6 of 11

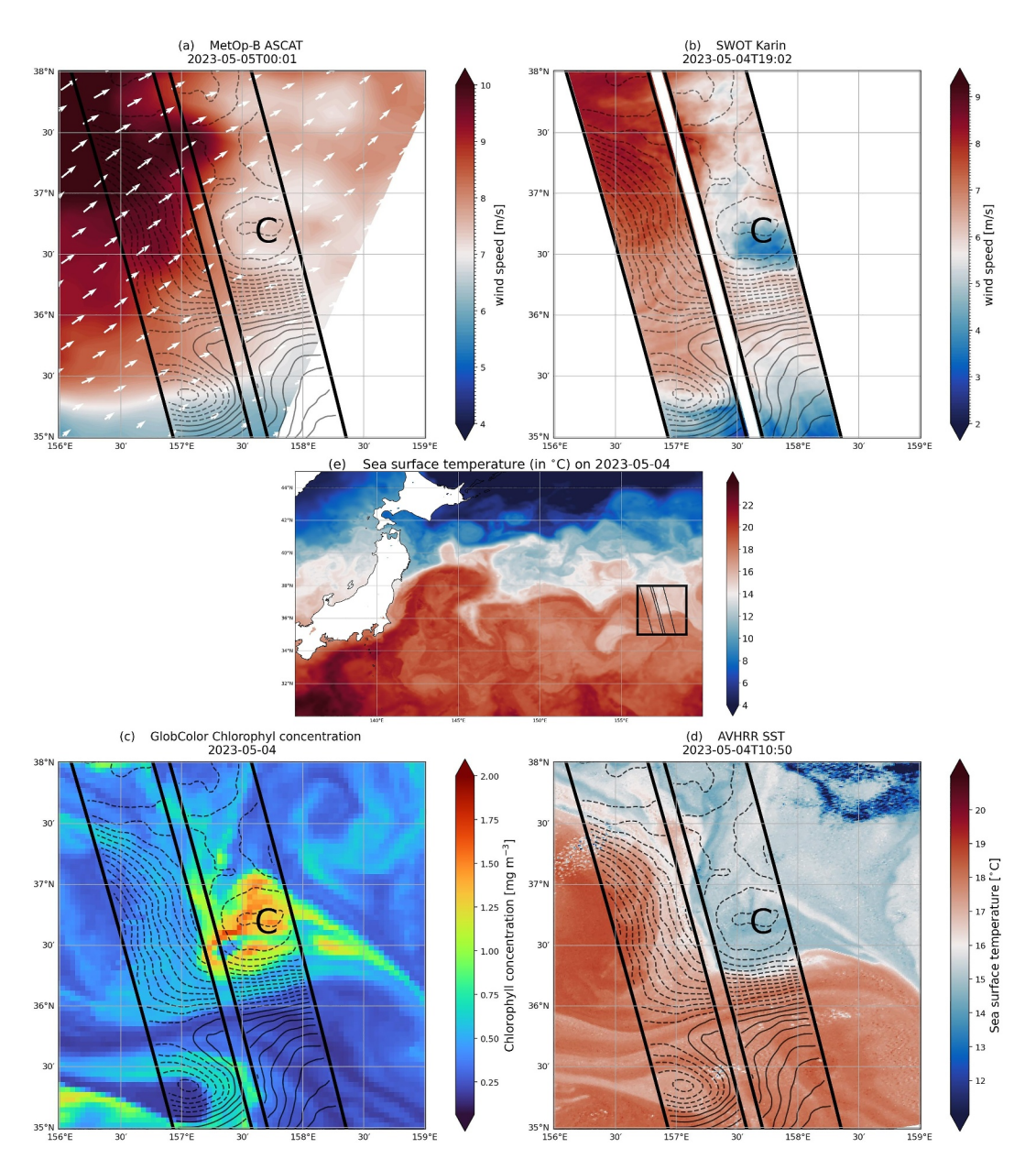


**Figure 3.** (a) MetOp-B ASCAT wind speeds on 5 May 2023 at 00:01 UTC (with wind vectors). (b) Surface Water and Ocean Topography (SWOT) wind speed on 4 May at 19:02 UTC. (c) Chlorophyll concentration from Copernicus-GlobColor, on 4 May. (d) AVHRR sea surface temperature (SST) on 4 May at 10:50 UTC. (e) Multiscale ultra-high-resolution (MUR) SST on 4 May. In panels (a–d) contours of absolute dynamic topography from SWOT are overlaid minus a constant value (continuous contours for anticyclonic anomalies, dashed ones for cyclonic ones). Note that the colorbars for the wind speeds of ASCAT and SWOT are different.

Another caveat is related to the process of retrieving the wind field from the instrument. SST has a direct effect on the variation of the radar backscatter coefficient through its effect on the reflectivity of seawater (Vandemark et al., 2016). However the Geophysical Model Function (GMF) used to compute surface winds from backscatter does not include this effect (Stiles et al., 2024), which may distort our vision of a dynamical effect of SST on the MABL. Tran et al. (2023) studied the potential bias in wind speed using data from the AltiKa altimeter which is also a Ka-band interferometer. From their Figure 1, we can estimate a bias of 0.05 m s<sup>-1</sup>  $^{\circ}$ C<sup>-1</sup> due to the dependence of the GMF to SST. This value is much smaller than the wind/SST coefficient about 0.2–0.5 m s<sup>-1</sup>  $^{\circ}$ C<sup>-1</sup> found in our study. This builds confidence that the observed correspondence between SST and wind speed anomalies at fine scales can be attributed to the effect of air-sea coupling.

KAOUAH ET AL. 7 of 11

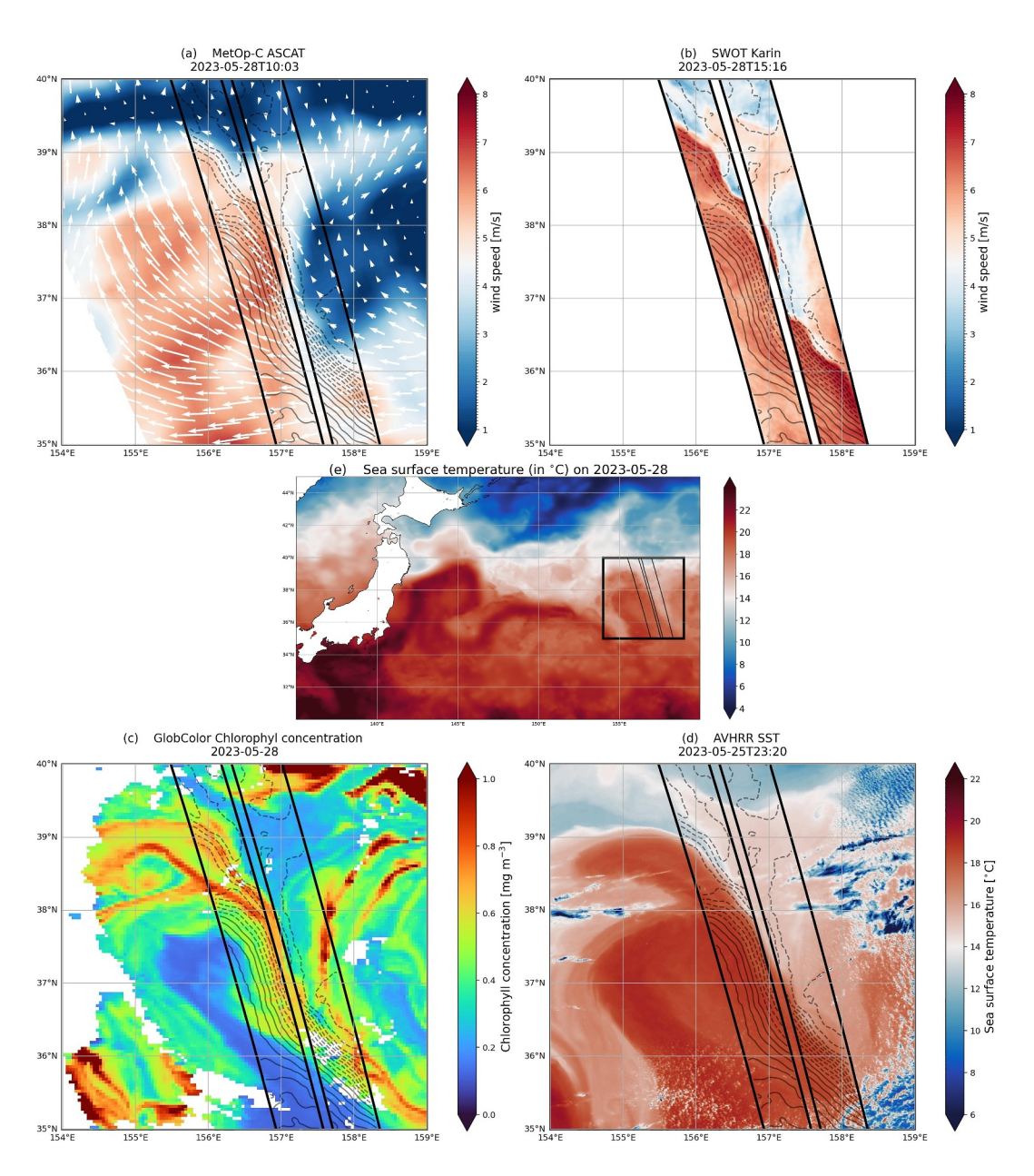


**Figure 4.** (a) MetOp-B ASCAT wind speeds on 28 May 2023 at 10:03 UTC (with wind vectors). (b) Surface Water and Ocean Topography (SWOT) wind speed on 28 May at 15:16 UTC. (c) Chlorophyll concentration from Copernicus-GlobColor, on 28 May. (d) AVHRR sea surface temperature (SST) on 25 May at 23:20 UTC. (e) MUR SST on 28 May. In panels (a–d) contours of absolute dynamic topography from SWOT are overlaid minus a constant value (continuous contours for anticyclonic anomalies and dashed ones for cyclonic ones).

Finally, contrary to scatterometers, SWOT does not provide the wind direction. As shown by O'Neill et al. (2010), spatial variation of wind direction is also affected by mesoscale SST gradients. As a result, SWOT data alone cannot be used to compute wind divergence and wind curl in order to examine their correlation with down-wind and cross-wind SST gradients. New missions such as ODYSEA (Larrañaga et al., 2025; Rodríguez et al., 2018; Torres et al., 2023) and analysis of the data of DopplerScat from the S-MODE campaign (Wineteer et al., 2024) could help to investigate these questions for meso and submesoscales.

## **Data Availability Statement**

The SWOT products used in this manuscript are freely distributed by mirror centers from NASA and CNES.

KAOUAH ET AL. 8 of 11

loi/10.1029/2025GL116017 by Ecole Normak

Wiley Online Library on [21/10/2025]. See

The SWOT Level 2 KaRin Low Rate Wind Wave Data Product is available in SWOT Project (2023). The product quality is not final and will be affected by some evolutions as the SWOT project team makes progress on science data processing algorithms and instrument calibrations. The SWOT Level 3 KaRin Low Rate Sea Surface Height Data Unsmoothed Data Product is available in AVISO/DUACS (2024). It is made freely available by AVISO and DUACS teams as part of the DESMOS Science Team project.

MetOp-B ASCAT winds products are provided by EUMETSAT/OSI SAF (2018). The SST data is provided by Group for High Resolution Sea Surface Temperature (GHRSST) and the National Oceanic and Atmospheric Administration (NOAA/STAR, 2023; JPL MUR MEaSUREs Project, 2015). The Copernicus-GlobColour product was obtained from the Copernicus Marine Service repository (2024).

All data sets were last accessed on 07 June 2025.

#### Acknowledgments

This work is a contribution to the joint projects I-CASCADE and POSEIDON funded by the French CNES TOSCA program. M. K. is supported by a PhD Grant funded by CNES and Sorbonne Université. We acknowledge CNES for awarding access to its HPC resources.

#### References

- Archer, M., Wang, J., Klein, P., Dibarboure, G., & Fu, L.-L. (2025). Wide-swath satellite altimetry unveils global submesoscale ocean dynamics. Nature, 640(8059), 691–696. https://doi.org/10.1038/s41586-025-08722-8
- AVISO/DUACS. (2024). Level-3 KaRIn low rate SSH unsmoothed (v1.0.1) [Dataset]. https://doi.org/10.24400/527896/A01-2024.003
- Bai, Y., Thompson, A. F., Villas-Bôas, A. B., Klein, P., Torres, H. S., & Menemenlis, D. (2023). Sub-mesoscale wind-front interactions: The combined impact of thermal and current feedback. Geophysical Research Letters, 50, e2023GL104807. https://doi.org/10.1029/2023GL104807
- Callies, J., Ferrari, R., Klymak, J. M., & Gula, J. (2015). Seasonality in submesoscale turbulence. *Nature Communications*, 6(1), 6862. https://doi.org/10.1038/ncomms/7862
- Capet, X., Mcwilliams, J. C., Molemaker, M. J., & Shchepetkin, A. F. (2008). Mesoscale to submesoscale transition in the California current system. Part III: Energy balance and flux. *Journal of Physical Oceanography*, 38(10), 2256–2269. https://doi.org/10.1175/2008jpo3810.1
- Chelton, D. B., Esbensen, S. K., Schlax, M. G., Thum, N., Freilich, M. H., Wentz, F. J., et al. (2001). Observations of coupling between surface wind stress and sea surface temperature in the eastern tropical Pacific. *Journal of Climate*, 14(7), 1479–1498. https://doi.org/10.1175/1520-0442(2001)014<1479:oocbsw>2.0.co;2
- Conejero, C., Renault, L., Desbiolles, F., McWilliams, J. C., & Giordani, H. (2024). Near-surface atmospheric response to meso- and sub-mesoscale current and thermal feedbacks. *Journal of Physical Oceanography*, 54(3), 823–848. https://doi.org/10.1175/jpo-d-23-0211.1
- Copernicus Marine Service repository. (2024). Copernicus-GlobColour [Dataset]. CMEMS. https://doi.org/10.48670/moi-00280 Czaja, A., Frankignoul, C., Minobe, S., & Vannière, B. (2019). Simulating the midlatitude atmospheric circulation: What might we gain from high-resolution modeling of air-sea interactions? Current Climate Change Reports, 5(4), 390–406. https://doi.org/10.1007/s40641-019-
- 00148-5
  EUMETSAT/OSI SAF. (2018). MetOp-B ASCAT level 2 ocean surface wind vectors optimized for coastal ocean [Dataset]. Version Operational/
- Near-Real-Time. https://doi.org/10.15770/EUM\_SAF\_OSI\_NRT\_2018

  Fu, L.-L., Pavelsky, T., Cretaux, J.-F., Morrow, R., Farrar, J. T., Vaze, P., et al. (2024). The surface water and ocean topography mission: A breakthrough in radar remote sensing of the ocean and land surface water. Geophysical Research Letters, 51(4), e2023GL107652. https://doi.org/10.1029/2023g1107652
- Gaube, P., Chickadel, C. C., Branch, R., & Jessup, A. (2019). Satellite observations of SST-induced wind speed perturbation at the oceanic submesoscale. Geophysical Research Letters, 46(5), 2690–2695. https://doi.org/10.1029/2018gl080807
- Gula, J., Molemaker, M. J., & McWilliams, J. C. (2014). Submesoscale cold filaments in the Gulf Stream. *Journal of Physical Oceanography*, 44(10), 2617–2643. https://doi.org/10.1175/jpo-d-14-0029.1
- Hayes, S. P., McPhaden, M. J., & Wallace, J. M. (1989). The influence of sea surface temperature on surface wind in the eastern equatorial Pacific: Weekly to monthly variability. *Journal of Climate*, 2(12), 1500–1506. https://doi.org/10.1175/1520-0442(1989)002<1500:tiosst>2.0.co;2
- Josey, S. A., Kent, E. C., & Taylor, P. K. (1999). New insights into the ocean heat budget closure problem from analysis of the SOC air–sea flux climatology. *Journal of Climate*, 12(9), 2856–2880. https://doi.org/10.1175/1520-0442(1999)012<2856:niitoh> 2.0.co:2
- JPL D-105502. (2023). SWOT algorithm theoretical basis Document: Level-2 KaRIn low rate sea surface height (L2\_LR\_SSH) science algorithm software. Jet Propulsion Laboratory Internal Document.
- JPL MUR MEaSUREs Project. (2015). GHRSST level 4 MUR global foundation sea surface temperature analysis. Ver. 4.1 [Dataset]. PO.DAAC. https://doi.org/10.5067/GHGMR-4FJ04
- Kilpatrick, T., Schneider, N., & Qiu, B. (2016). Atmospheric response to a midlatitude SST front: Alongfront winds. *Journal of the Atmospheric*
- Sciences, 73(9), 3489–3509. https://doi.org/10.1175/jas-d-15-0312.1 Klein, P., Hua, B. L., Lapeyre, G., Capet, X., Le Gentil, S., & Sasaki, H. (2008). Upper ocean turbulence from high 3-D resolution simulations.
- Journal of Physical Oceanography, 38(8), 1748–1763. https://doi.org/10.1175/2007jpo3773.1 Klein, P., & Lapeyre, G. (2009). The oceanic vertical pump induced by mesoscale and submesoscale turbulence. Annual Review of Marine
- Science, 1, 351–375. https://doi.org/10.1146/annurev.marine.010908.163704

  Klein, P., Lapeyre, G., Siegelman, L., Qiu, B., Fu, L.-L., Torres, H., et al. (2019). Ocean scale interactions from space. Earth and Space Science, 6(5), 795–817. https://doi.org/10.1029/2018ea000492
- Larrañaga, M., Renault, L., Wineteer, A., Contreras, M., Arbic, B. K., Bourassa, M. A., & Rodriguez, E. (2025). Assessing the future ODYSEA satellite mission for the estimation of ocean surface currents, wind stress, energy fluxes, and the mechanical coupling between the ocean and the atmosphere. Remote Sensing, 17(2), 302. https://doi.org/10.3390/rs17020302
- Lévy, M., Franks, P. J. S., & Smith, K. S. (2018). The role of submesoscale currents in structuring marine ecosystems. *Nature Communications*, 9(1), 4758, https://doi.org/10.1038/s41467-018-07059-3
- Lindzen, R. S., & Nigam, S. (1987). On the role of sea surface temperature gradients in forcing low level winds and convergence in the tropics. Journal of the Atmospheric Sciences, 44(17), 2418–2436. https://doi.org/10.1175/1520-0469(1987)044<2418:otross>2.0.co;2
- Ma, J., Xu, H. M., Dong, C. M., Lin, P. F., & Liu, Y. (2015). Atmospheric responses to oceanic eddies in the Kuroshio Extension region. *Journal of Geophysical Research: Atmospheres*, 120(13), 6313–6330. https://doi.org/10.1002/2014jd022930

KAOUAH ET AL. 9 of 11

- McWilliams, J. C. (2016). Submesoscale currents in the ocean. *Proceedings of the Royal Society A: Mathematical, Physical and Engineering Sciences*, 472(2189), 20160117. https://doi.org/10.1098/rspa.2016.0117
- Morrow, R., Fu, L.-L., Ardhuin, F., Benkiran, M., Chapron, B., Cosme, E., et al. (2019). Global observations of fine-scale ocean surface topography with the surface water and ocean topography (SWOT) mission. Frontiers in Marine Science, 6, 232. https://doi.org/10.3389/fmars. 2019.00232
- NOAA/STAR. (2023). GHRSST L2P Metop-C AVHRR FRAC ACSPO v2.80 1km dataset. Ver. 2.80 [Dataset]. PO.DAAC. https://doi.org/10.5067/GHMTC-2PS28
- Nuijens, L., Wenegrat, J., Lopez Dekker, P., Pasquero, C., O'Neill, L. W., Ardhuin, F., et al. (2024). *The air-sea interaction (ASI) submesoscale:*Physics and impact. White-paper from the Lorentz-Center Workshop on 'Ocean-atmosphere coupling at (sub)mesoscales', in Leiden, the Netherlands, September 2023. https://doi.org/10.5065/78ac-qd31
- O'Neill, L. W. (2012). Wind speed and stability effects on coupling between surface wind stress and SST observed from buoys and satellite. Journal of Climate, 25(5), 1544–1569. https://doi.org/10.1175/jcli-d-11-00121.1
- O'Neill, L. W., Chelton, B., & Esbensen, S. K. (2010). The effects of SST-induced surface wind speed and direction gradients on midlatitude surface vorticity and divergence. *Journal of Climate*, 23(2), 255–281. https://doi.org/10.1175/2009jcli2613.1
- O'Neill, L. W., Chelton, D. B., Esbensen, S. K., & Wentz, F. J. (2005). High-resolution satellite measurements of the atmospheric boundary layer response to SST variations along the Agulhas return current. *Journal of Climate*, 18(14), 2706–2723. https://doi.org/10.1175/jcli3415.1
- Peral, E., Esteban-Fernández, D., Rodríguez, E., McWatters, D., De Bleser, J.-W., Ahmed, R., et al. (2024). KaRIn, the Ka-band radar interferometer of the SWOT mission: Design and in-flight performance. *IEEE Transactions on Geoscience and Remote Sensing*, 62, 1–27. https://doi.org/10.1109/tgrs.2024.3405343
- Qiu, B. (2003). Kuroshio Extension variability and forcing of the Pacific decadal oscillations: Responses and potential feedback. *Journal of Physical Oceanography*, 33(12), 2465–2482. https://doi.org/10.1175/1520-0485(2003)033<2465:KEVAFO>2.0.CO;2
- Qiu, B., Nakano, T., Chen, S., & Klein, P. (2017). Submesoscale transition from geostrophic flows to internal waves in the northwestern Pacific upper ocean. *Nature Communications*, 8(1), 14055. https://doi.org/10.1038/ncomms14055
- Renault, L., Contreras, M., Marchesiello, P., Conejero, C., Uchoa, I., & Wenegrat, J. (2024). Unraveling the impacts of submesoscale thermal and current feedbacks on the low-level. Winds and oceanic submesoscale currents. *Journal of Physical Oceanography*, 54(12), 2463–2486. https://doi.org/10.1175/jpo-d-24-0097.1
- Renault, L., Masson, S., Oerder, V., Jullien, S., & Colas, F. (2019). Disentangling the mesoscale ocean-atmosphere interactions. *Journal of Geophysical Research: Oceans*, 124(3), 2164–2178. https://doi.org/10.1029/2018jc014628
- Renault, L., Molemaker, M. J., McWilliams, J. C., Shchepetkin, A. F., Lemarié, F., Chelton, D., et al. (2016). Modulation of wind work by oceanic current interaction with the atmosphere. *Journal of Physical Oceanography*, 46(6), 1685–1704. https://doi.org/10.1175/jpo-d-15-0232.1
- Rodríguez, E., Wineteer, A., Perkovic-Martin, D., Gál, T., Stiles, B. W., Niamsuwan, N., & Rodríguez Monje, R. (2018). Estimating ocean vector winds and currents using a Ka-band pencil-beam Doppler scatterometer. *Remote Sensing*, 10(4), 576. https://doi.org/10.3390/rs10040576
- Scharffenberg, M., & Stammer, D. (2010). Seasonal variations of the large-scale geostrophic flow field and eddy kinetic energy inferred from the TOPEX/Poseidon and Jason-1 tandem mission data. *Journal of Geophysical Research*, 115(C2), C02008. https://doi.org/10.1029/2008ic005242
- Shao, M., Ortiz-Suslow, D. G., Haus, B. K., Lund, B., Williams, J. N., Özgökmen, T. M., et al. (2019). The variability of winds and fluxes observed near submesoscale fronts. *Journal of Geophysical Research: Oceans*, 124, 7756–7780. https://doi.org/10.1029/2019JC015236
- Shao, M., & Wu, L. (2024). Atmospheric fronts shaping the (sub)mesoscale SST-wind coupling over the Southern Ocean: Observational case. Journal of Geophysical Research: Atmospheres, 129(8), e2023JD039386. https://doi.org/10.1029/2023jd039386
- Song, X., Xie, X., Qiu, B., Cao, H., Xie, S.-P., Chen, Z., & Yu, W. (2022). Air-sea latent heat flux anomalies induced by oceanic submesoscale processes: An observational case study. Frontiers in Marine Science, 9, 850207. https://doi.org/10.3389/fmars.2022.850207
- Stiles, B. W., Fore, A. G., Bohe, A., Chen, A. C., Chen, C. W., Molero, B., & Dubois, P. (2024). Ocean surface wind speed retrieval for SWOT Kaband radar interferometer. In *IGARSS 2024 2024 IEEE international geoscience and remote sensing symposium* (pp. 1422–1425). https://doi.org/10.1109/IGARSS53475.2024.10640472
- Strobach, E., Klein, P., Molod, A., Fahad, A. A., Trayanov, A., Menemenlis, D., & Torres, H. (2022). Local air-sea interactions at ocean mesoscale in western boundary currents. *Geophysical Research Letters*, 49(7), e2021GL097003. https://doi.org/10.1029/2021gl097003
- Su, Z., Wang, J., Klein, P., Thompson, A. F., & Menemenlis, D. (2018). Ocean submesoscales as a key component of the global heat budget. Nature Communications, 9(1), 775. https://doi.org/10.1038/s41467-018-02983-w
- Sublette, M. S., & Young, G. S. (1996). Warm-season effects of the Gulf Stream on mesoscale characteristics of the atmospheric boundary layer. Monthly Weather Review, 124, 653–667. https://doi.org/10.1175/1520-0493(1996)124<0653:WSEOTG>2.0.CO;2
- Sullivan, P. P., & McWilliams, J. C. (2022). Atmospheric boundary layers over an oceanic eddy. *Journal of the Atmospheric Sciences*, 79(10), 2601–2620. https://doi.org/10.1175/jas-d-22-0019.1
- Sullivan, P. P., McWilliams, J. C., Weil, J. C., Patton, E. G., & Fernando, H. J. S. (2021). Marine boundary layers above heterogeneous SST: Alongfront winds. *Journal of the Atmospheric Sciences*, 78(10), 3297–3315. https://doi.org/10.1175/jas-d-21-0072.1
- SWOT Project. (2023). Level-2 KaRIn low rate WindWave (v2.0) [Dataset]. https://doi.org/10.24400/527896/A01-2023.014
- Taylor, J. R., & Thompson, A. F. (2023). Submesoscale dynamics in the upper ocean. Annual Review of Fluid Mechanics, 55(1), 103–127. https://doi.org/10.1146/annurev-fluid-031422-095147
- Torres, H., Wineteer, A., Klein, P., Lee, T., Wang, J., Rodriguez, E., et al. (2023). Anticipated capabilities of the ODYSEA wind and current mission concept to estimate wind work at the air–sea interface. *Remote Sensing*, 15(13), 3337. https://doi.org/10.3390/rs15133337
- Tran, N., Vandemark, D., Bignalet-Cazalet, F., & Dibarboure, G. (2023). Quantifying multifrequency ocean altimeter wind speed errors due to sea surface temperature and resulting impacts on satellite sea level measurements. *Remote Sensing*, 15(13), 3235. https://doi.org/10.3390/rs15133235
- Vandemark, D., Chapron, B., Feng, H., & Mouche, A. (2016). Sea surface reflectivity variation with ocean temperature at Ka-band observed using near-nadir satellite radar data. *IEEE Geoscience and Remote Sensing Letters*, 13(4), 510–514. https://doi.org/10.1109/lgrs.2016.2520823
- Verhoef, A., Portabella, M., & Stoffelen, A. (2012). High-resolution ASCAT scatterometer winds near the coast. *IEEE Transactions on Geoscience and Remote Sensing*, 50(7), 2481–2487. https://doi.org/10.1109/tgrs.2011.2175001
- Vivant, F., Siegelman, L., Klein, P., Torres, H. S., Menemenlis, D., & Molod, A. M. (2025). Ocean submesoscale fronts induce diabatic heating and convective precipitation within storms. Communications Earth & Environment, 6(1), 69. https://doi.org/10.1038/s43247-025-02002-z
- Vogelzang, J., Stoffelen, A., Lindsley, R. D., Verhoef, A., & Verspeek, J. (2017). The ASCAT 6.25-km wind product. IEEE Journal of Selected Topics in Applied Earth Observations and Remote Sensing, 10(5), 2321–2331. https://doi.org/10.1109/jstars.2016.2623862

KAOUAH ET AL. 10 of 11



# **Geophysical Research Letters**

- 10.1029/2025GL116017
- Wallace, J. M., Mitchell, T. P., & Deser, C. (1989). The influence of sea surface temperature on surface wind in the eastern equatorial Pacific: Seasonal and interannual variability. *Journal of Climate*, 2(12), 1492–1499. https://doi.org/10.1175/1520-0442(1989)002<1492:tiosst>2.0.
- Wenegrat, J. O., & Arthur, R. S. (2018). Response of the atmospheric boundary layer to submesoscale sea-surface temperature fronts. *Geophysical Research Letters*, 45(24), 13505–13512. https://doi.org/10.1029/2018g1081034
- Wineteer, A., Rodriguez, E., Martin, D. P., Torres, H., Polverari, F., Akbar, R., & Rocha, C. (2024). Exploring the characteristics of ocean surface winds at high resolution with doppler scatterometry. *Geophysical Research Letters*, 51(23), e2024GL113455. https://doi.org/10.1029/2024gl113455
- Zhang, Z., Miao, M., Qiu, B., Tian, J., Jing, Z., Chen, G., & Zhao, W. (2024). Submesoscale eddies detected by SWOT and moored observations in the Northwestern Pacific. *Geophysical Research Letters*, 51(15), e2024GL110000. https://doi.org/10.1029/2024gl110000

KAOUAH ET AL. 11 of 11

#### GEOPHYSICAL RESEARCH LETTERS

# Supporting Information for "Submesoscale air-sea interactions as revealed by SWOT"

M. Kaouah<sup>1,2</sup>, G. Lapeyre<sup>1</sup>, L. Renault<sup>2</sup>, X. Perrot<sup>1</sup>and C. Dablemont<sup>3</sup>

<sup>1</sup>LMD-IPSL, ENS, Université PSL, Sorbonne Université, CNRS, Paris, France

<sup>2</sup>Université de Toulouse, LEGOS (CNES/CNRS/IRD/UPS), Toulouse, France

<sup>3</sup>Institut des Sciences Moléculaires d'Orsay (ISMO), CNRS, Université Paris-Saclay, France

#### Contents of this file

### 1. Data description

Through the article, we use the L2 product (PGC0, as of 07/07/2025), which provides 10-m equivalent neutral wind (ENW) speed relative to the surface current with a nominal resolution of 2 km (JPL D-56407, Revision C, 2025). Note that wind directions cannot be retrieved as the measurements are acquired from a single azimuth. The Gulf Stream data (on May 12, 2023, approximately at 22:20) correspond to pass 9, cycle 519 of the

Corresponding author: G. Lapeyre, LMD-IPSL, Ecole Normale Supérieure, 75005 Paris, France. (guillaume.lapeyre@sorbonne-universite.fr)

1-day repeat period of the SWOT mission, which occurred between March 29 and July 11, 2023.

The scatterometer measurements come from the MetOp-B ASCAT-L2-Coastal products (OSI/SAF, 2021) which also provide 10 m ENW relative to the surface current with a nominal resolution of 12.5 km. Only a few snapshots were available in the time range ±12h from the SWOT measurements, one at 15:17 UTC on May 12 and one at 2:35 UTC on May 13.

The AVHRR SST data come from NOAA's Advanced Very High Resolution Radiometer (AVHRR L2p) with a nominal resolution of 1.1 km at nadir (NOAA/STAR, 2023). The MUR SST data were provided by JPL under support by NASA MEaSUREs program on a global resolution  $0.01^{\circ} \times 0.01^{\circ}$  (JPL MUR MEaSUREs Project, 2015).

Finally, for visual comparison, we also examine Chlorophyll concentration from the 4 km resolution L3 daily product Copernicus-GlobColor (Copernicus Marine Service repository, 2024).

1. Figures S1 to S3.

#### References

Copernicus Marine Service repository. (2024). Copernicus-GlobColour [[Dataset] CMEMS]. doi: 10.48670/moi-0028

JPL D-56407, Revision C. (2025). SWOT Product Description Document:, Level-2 KaRIn Low Rate Sea Surface Height L2\_LR\_SSH Data Product. Jet Propulsion Laboratory Internal Document.

JPL MUR MEaSUREs Project. (2015). GHRSST Level 4 MUR Global Foundation

- Sea Surface Temperature Analysis. Ver. 4.1. PO.DAAC, CA, USA. [Dataset]. doi: 10.5067/GHGMR-4FJ04
- NOAA/STAR. (2023). GHRSST L2P Metop-C AVHRR FRAC ACSPO v2.80 1km

  Dataset. Ver. 2.80. PO.DAAC, CA, USA [Dataset]. doi: 10.5067/GHMTC-2PS28

  OSI/SAF. (2021). ASCAT Wind Product User Manual,

  SAF/OSI/CDOP/KNMI/TEX/MA/126.

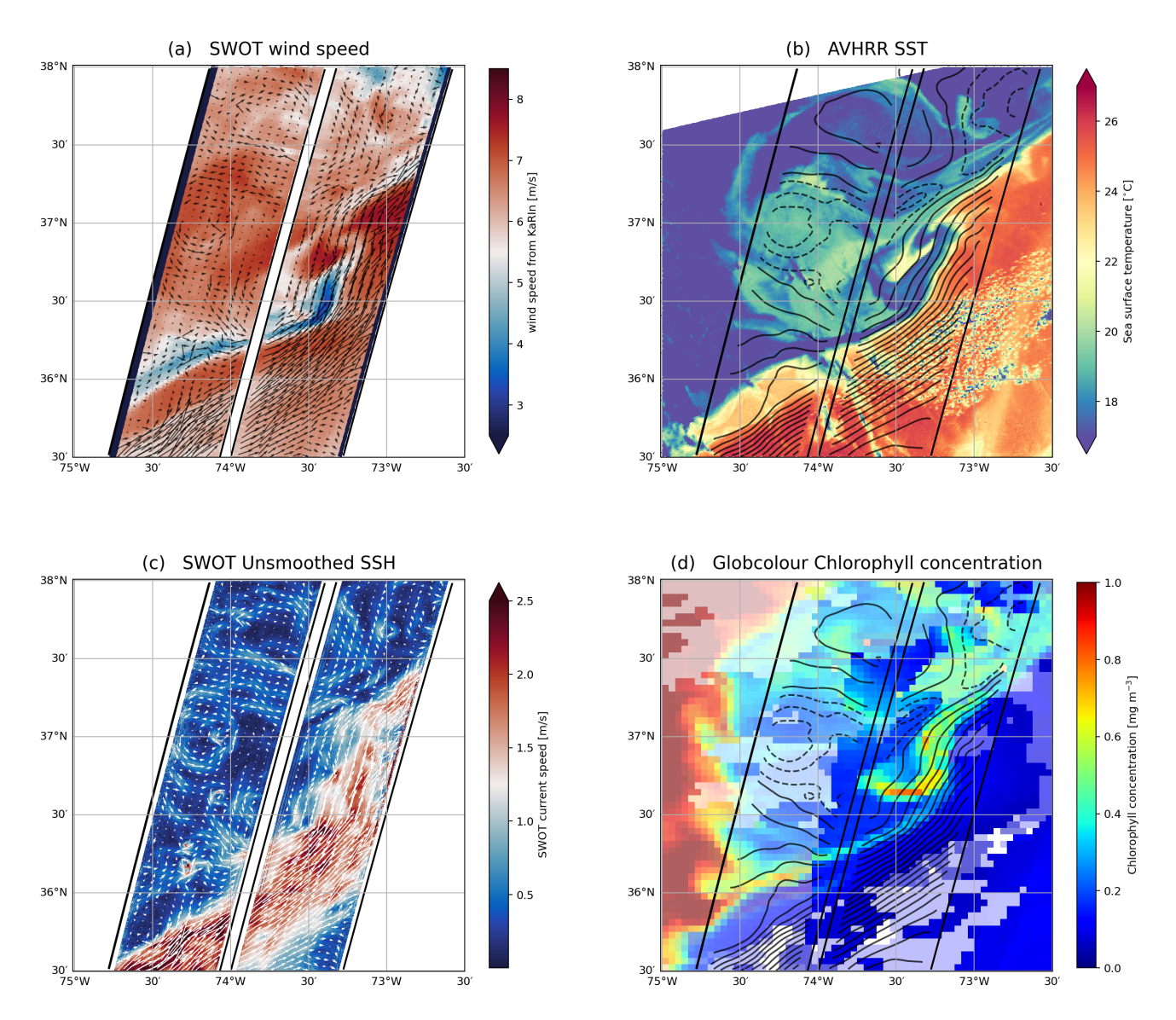
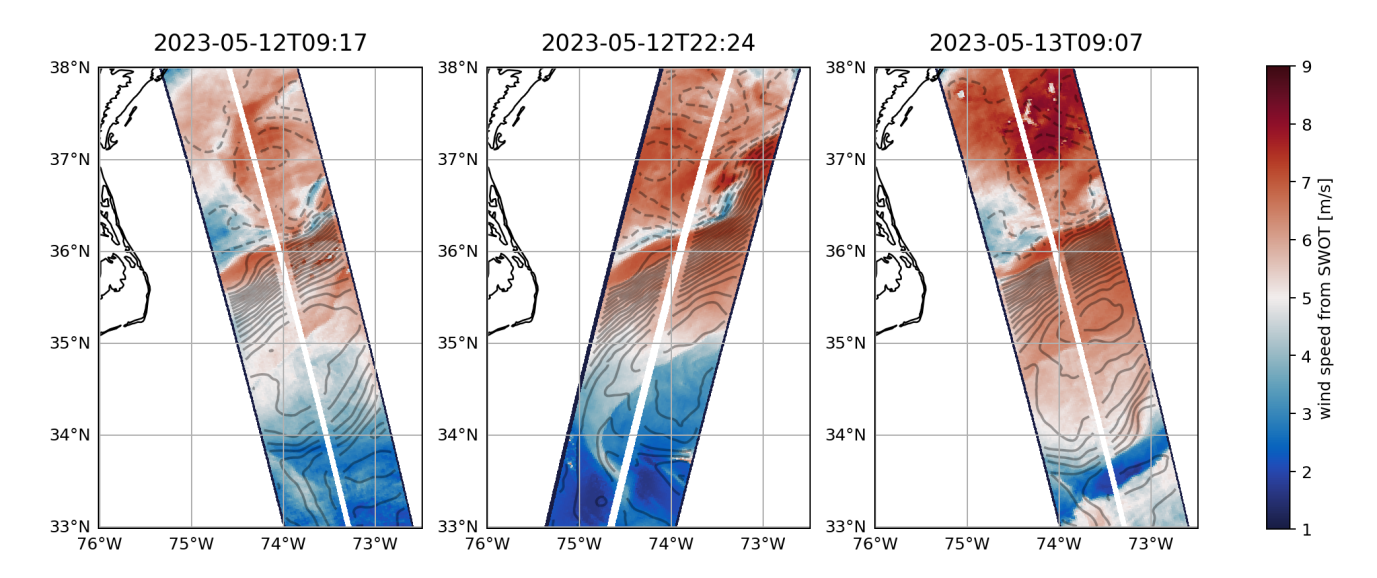
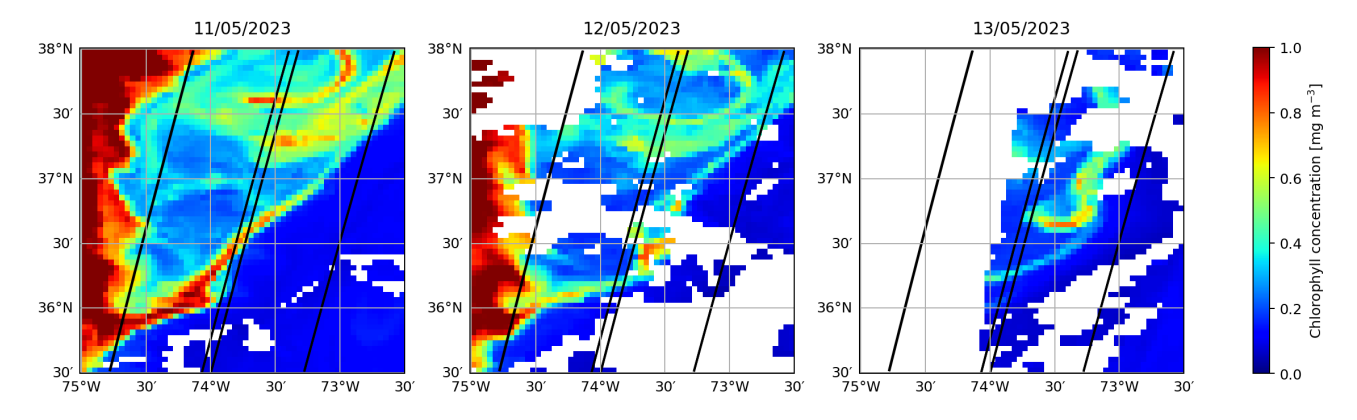


Figure S1. A close-up of different quantities near the cold pouch at 36.5°N, 73.5°W. (a) SWOT wind speed; (b) AVHRR SST. (c) SWOT "Unsmoothed" (250 m) ocean currents. (d) Globcolour Chlorophyll concentration using different snapshots (see Fig. S3). In (a) and (c), vectors correspond to ocean currents from SWOT Unsmoothed product. In (b) and (d), black contours correspond to SWOT SSH. Black lines represent the swaths of the satellite.



**Figure S2.** Evolution of wind speed as seen by SWOT. SSH anomalies are overlaid. The weaker wind speed associated to the cold filament persists over 1 day.



**Figure S3.** Chlorophyll concentration at different times, used to produce Fig. 1c of the paper and Fig. S1b.